

AD-A174 491

MULTISCATTERING LIDAR METHOD FOR DETERMINING OPTICAL  
PARAMETERS OF AEROSOLS(U) DEFENCE RESEARCH  
ESTABLISHMENT VALCARTIER (QUEBEC) L R BISSONNETTE

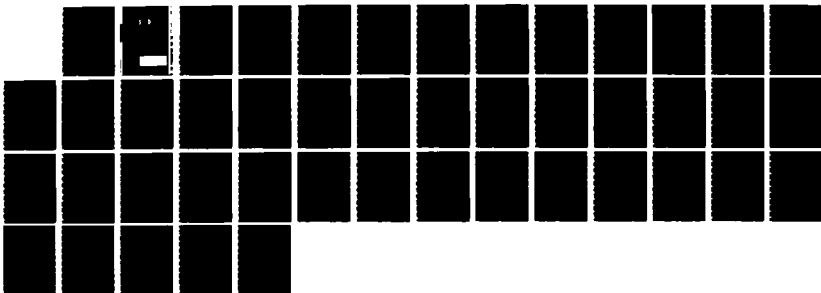
1/1

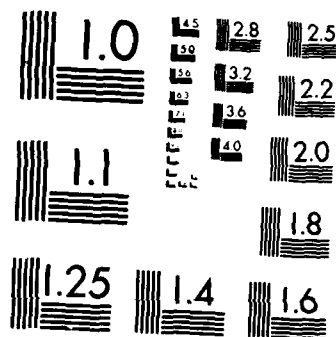
UNCLASSIFIED

OCT 86 DREV-4430/86

F/G 7/4

NL





MICROCOPY RESOLUTION TEST CHART  
NATIONAL BUREAU OF STANDARDS 1963-A



National Defence  
Défense nationale

3

UNCLASSIFIED  
UNLIMITED DISTRIBUTION

DREV REPORT 4430/86  
FILE: 3633B-015  
OCTOBER 1986

CRDV RAPPORT 4430/86  
DOSSIER: 3633B-015  
OCTOBRE 1986

DTIC  
ELECTE  
NOV 26 1986  
S D

MULTISCATTERING LIDAR METHOD FOR DETERMINING  
OPTICAL PARAMETERS OF AEROSOLS

L.R. Bissonnette

AD-A174 491

DTIC FILE COPY

RESEARCH AND DEVELOPMENT BRANCH  
DEPARTMENT OF NATIONAL DEFENCE  
CANADA

BUREAU - RECHERCHE ET DÉVELOPPEMENT  
MINISTÈRE DE LA DÉFENSE NATIONALE  
CANADA

Defence Research Establishment  
Centre de recherches pour la Défense,  
Valcartier, Québec

Canada

SANS CLASSIFICATION  
DISTRIBUTION ILLIMITÉE

86 11 25 278

DREV R-4430/86  
FILE: 3633B-015

UNCLASSIFIED

CRDV R-4430/86  
DOSSIER: 3633B-015

MULTISCATTERING LIDAR METHOD FOR DETERMINING  
OPTICAL PARAMETERS OF AEROSOLS

by

L.R. Bissonnette

DEFENCE RESEARCH ESTABLISHMENT  
CENTRE DE RECHERCHES POUR LA DÉFENSE  
VALCARTIER

Tel: ('18) 844-4271

Québec, Canada

October/octobre 1986

SANS CLASSIFICATION

ABSTRACT

A new lidar technique is proposed for determining aerosol optical parameters. It consists in recording the lidar returns at three fields of view to measure the differences caused by multiple scatterings. The inversion algorithm uses that information to obtain the aerosol forward-scattering coefficient through simple algebraic formulas. Sample solutions are calculated for simulated lidar signals and compared with the results derived from the standard single-scattering lidar equation. The agreement with the true values is very good and performance is consistently better than, or at least as good as, that of the single-scattering method. The proposed technique requires neither a boundary value nor a backscatter-to-extinction relation, which makes such lidar measurements completely self-sufficient for the remote determination of the range-resolved forward-scattering coefficient of atmospheric aerosols.

RÉSUMÉ

Une nouvelle technique lidar pour la détermination de paramètres optiques des aérosols est proposée. Elle consiste à enregistrer les rétrodiffusions lidar sous trois champs de vision angulaire pour mesurer les différences provenant des diffusions multiples. L'algorithme d'inversion utilise ces données pour obtenir par des opérations algébriques simples le coefficient de diffusion vers l'avant des aérosols. Des exemples de calcul sont effectués pour des signaux lidar simulés et comparés aux résultats obtenus à partir de l'équation du lidar en diffusion simple. Le recouplement avec les valeurs exactes est très bon et les performances sont meilleures ou du moins aussi bonnes que celles de la méthode de diffusion simple. La méthode suggérée requiert ni valeur aux limites ni relation entre les coefficients d'extinction et de rétrodiffusion, ce qui la rend tout à fait autosuffisante pour déterminer à distance la distribution spatiale du coefficient de diffusion vers l'avant des aérosols atmosphériques.



Accession For	
NTIS CRA&I	<input checked="" type="checkbox"/>
DTIC TAB	<input type="checkbox"/>
Unannounced	<input type="checkbox"/>
Justification	
By	
Distribution /	
Availability Codes	
Dist	Avail and/or Special
A-1	

TABLE OF CONTENTS

ABSTRACT/RÉSUMÉ .....	1
1.0 INTRODUCTION .....	1
2.0 LIDAR SIMULATION .....	2
2.1 Model .....	2
2.2 Cloud Specifications .....	4
3.0 SINGLE-SCATTERING LIDAR INVERSION .....	8
3.1 Solution Methods .....	8
3.2 Results .....	11
4.0 MULTISCATTERING INVERSION METHOD .....	23
4.1 Solution Method .....	23
4.2 Results .....	30
5.0 SUMMARY AND CONCLUSIONS .....	36
6.0 REFERENCES .....	39
FIGURES 1 to 22	

## 1.0 INTRODUCTION

A major characteristic of modern defence systems is the use of electro-optic (EO) devices for search, detection, tracking, guidance and control. The performance of these systems is very good in clear visibility but it can be severely degraded by poor weather conditions, especially by the presence of aerosol particles. The principal difficulty in the tactical deployment of these systems is the great variability of aerosol composition and concentration, which makes performance assessment at any time in any weather very unreliable. Therefore, there is a need for an instrument that could remotely measure in real time and in situ the aerosol extinction coefficient in the immediate environment where the EO systems are to be deployed.

Lidar appears as an attractive solution to this problem of determining the aerosol extinction coefficient in an inhomogeneous medium. However, the technique still involves a number of difficulties. The standard single-scattering lidar theory assumes that the detected photons have encountered only one scattering before being collected. Moreover, the solution method requires a relation between the backscatter and extinction coefficients, and the specification of a boundary value of the extinction coefficient, preferably at the outer end of the lidar range. These data cannot in general be derived from the measured lidar signals; most often, they are guessed or estimated through very limited independent information. Because of these problems, the single-scattering lidar solutions are subject to important errors and uncertainties (Refs. 1-5) that can make tactical application of lidar unfeasible under general weather conditions.

This report proposes a lidar technique that uses the information carried by the multiple-scattering contributions to relax the limitations imposed by the single-scattering equation. The method entails the simultaneous recording of lidar returns at three fields of view but it requires neither a boundary value nor a backscatter-to-extinction relation. The inversion algorithm is simple, it is similar to the well-known slope method but applied to the ratios of the lidar signals at the different fields of view. Sample calculations are performed with simulated signals and the results are promising. In a recent article, Sassen and Petrilla (Ref. 6) hinted that multiscattering contributions can indeed contain recoverable information.

Chapter 2.0 summarizes the method of generation of the simulated lidar signals. The resulting single-scattering lidar solutions are given and discussed in Chapter 3.0. Finally, Chapter 4.0 describes the proposed multiscattering lidar concept and discusses the solutions obtained.

This work was performed at DREV between January and May 1986 under PCN 33B15, Lidar Determination of Atmospheric Parameters.

## 2.0 LIDAR SIMULATION

### 2.1 Model

In analyzing the lidar solutions for the aerosol extinction coefficient, it is important to compare the results with the true coefficient. This is difficult to achieve experimentally since the lidar gives a range-resolved distribution of the extinction coefficient which contains information on a finer scale than generally available from independent simultaneous measurements. Transmittance data are useful but they give only the range-integrated extinction coefficient.

Vertical profiles of visibility and particle size distributions have been obtained during lidar experiments at the same site (Refs. 7 and 8). The visibility data can be transformed to extinction coefficients but the wavelength is different than that of the lidar. Similarly, extinction profiles can be calculated from the size distributions but the results are subject to unknown errors because of instrumental range limitations on particle sizes and uncertainties in the complex refractive index of the particles. Although such measurements are indispensable and constitute the ultimate test, they cannot provide detailed comparisons under varied conditions. A convenient alternative, suitable for comparing solution methods, is to numerically generate lidar signals for given profiles of extinction and backscatter coefficients. In most studies published to date (e.g. Refs. 1-4), the model used to compute the lidar signals is the single-scattering lidar equation itself. Hence, such practical effects as the dependence on the receiver field of view and multiscattering contributions cannot be analyzed.

For the present application, the lidar signals are generated through solutions of a multiscattering propagation model developed at DREV (Refs. 9 and 10). The model predicts the radiant intensities of the transmitted, forward- and backscattered radiation from a coherent laser beam directed into a particulate medium. The solutions can be calculated for inhomogeneous clouds and they take into account multiple scatterings. Validation was performed against laboratory data obtained at three wavelengths (0.63, 1.06 and 10.6  $\mu\text{m}$ ) in water droplet clouds (Ref. 10). The agreement is very good, especially for the backscatter solutions which are of interest here. The predictions also agree within 5% with Monte Carlo backscatter calculations carried out at 1.06, 3.5 and 10.5  $\mu\text{m}$  for various generic aerosol models (Ref. 10).

## 2.2 Cloud Specifications

The aerosol clouds are modeled from the Air Force Geophysics Laboratory (AFGL) generic rural, urban and maritime aerosols (Ref. 11). These aerosols are representative of atmospheric conditions. For the present application, they are mixed into various configurations to create a wide range of inhomogeneities. All clouds are assumed to be 1 km in depth.

The first cloud studied has a homogeneous composition, the maritime aerosol model at 99% relative humidity was chosen. This gives a ratio of the backscatter to extinction coefficients  $\beta/\alpha_e$  of 0.038 at the 1.06- $\mu\text{m}$  wavelength of the assumed lidar. The density is varied to give a saw tooth extinction profile, the extinction coefficient  $\alpha_e$  is 1  $\text{km}^{-1}$  at the cloud boundaries and 6  $\text{km}^{-1}$  at the center. The cloud optical depth is 3.5. Figure 1 shows the  $\alpha_e$  and  $\beta/\alpha_e$  profiles for this case.

The second cloud is made more complex by varying the aerosol composition to modulate the  $\beta/\alpha_e$  ratio. The spatial variation of this ratio constitutes an important difficulty for lidar inversion. Urban and maritime aerosols are mixed in decreasing and increasing proportion respectively over the first half of the cloud, and maritime and rural aerosols are similarly mixed over the second half. The particles are 100% urban at the near-end boundary, 100% maritime at the center and 100% rural at the far-end boundary. The relative humidity is 70% everywhere. This produces a  $\beta/\alpha_e$  at 1.06  $\mu\text{m}$  that linearly increases from 0.0096 to 0.0396 and then decreases to 0.0210. Thus, the  $\beta/\alpha_e$  ratio changes smoothly by a factor of approximately 4 in the first half, and 2 in the second half. The extinction profile is chosen the same as in Fig. 1. Figure 2 illustrates the  $\alpha_e$  and  $\beta/\alpha_e$  distributions for this case.

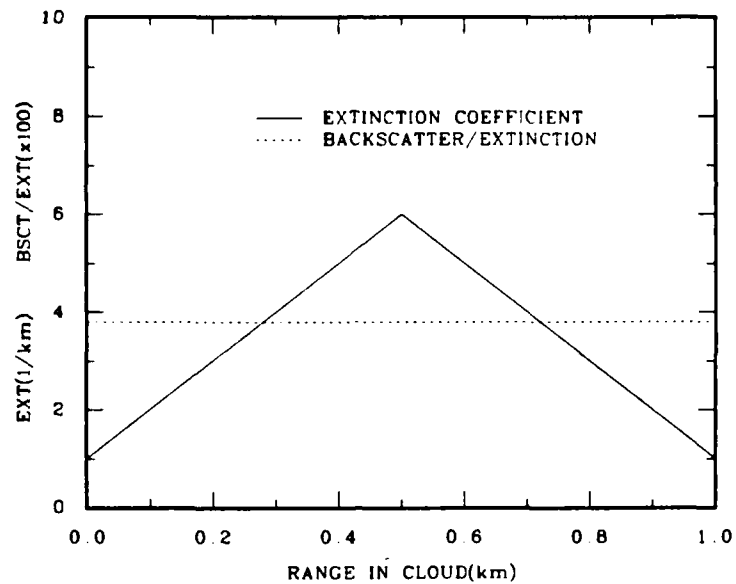


FIGURE 1 - Profiles of the extinction coefficient  $\alpha_e$  and backscatter-to-extinction ratio  $\beta/\alpha_e$  at a wavelength of  $1.06 \mu\text{m}$  for a 1-km deep cloud consisting of the generic maritime aerosol model (Ref. 11) at 99% relative humidity.

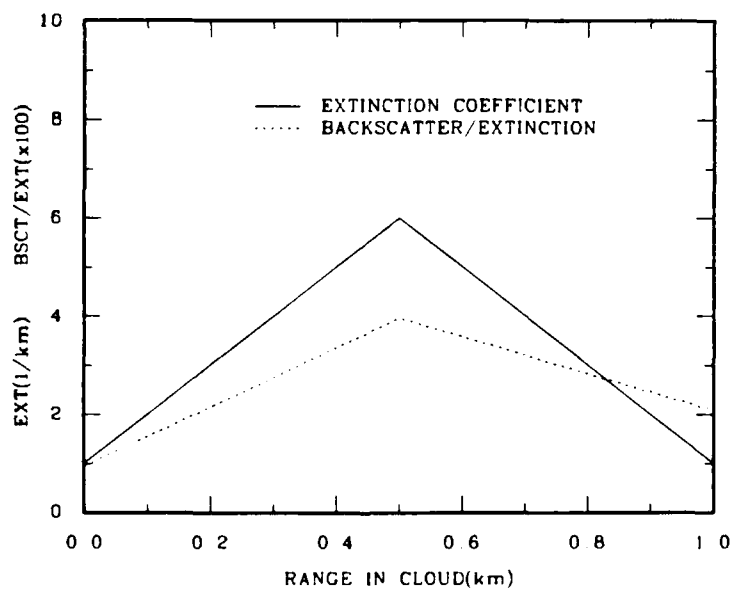


FIGURE 2 - Same as Fig. 1 but for a cloud consisting of a mixture of the generic urban, maritime and rural aerosol models (Ref. 11) at 70% relative humidity.

A more complex configuration is studied by juxtaposing regions of different aerosol composition. Figure 3 illustrates the structure. The three regions have each a saw tooth extinction profile but they are made respectively of urban, maritime and rural aerosols at 70% relative humidity. The  $\beta/\alpha_e$  ratio thus varies spatially in sharp steps from 0.0096, up to 0.0396 and down to 0.0210. The expected difficulty here is the more complex structure and the abrupt changes in the  $\beta/\alpha_e$  profile. Another example of similar complexity is shown in Fig. 4 where rural and maritime aerosols are made to alternate with varying concentrations.

The clouds depicted in Figs. 1-4 were not chosen to model specific or realistic conditions but to provide a range of variations for both the extinction coefficient and the backscatter-to-extinction ratio that can be representative of natural aerosols.

The lidar returns from these clouds are computed with the propagation model outlined in the preceding section. It is assumed that the transmitter and receiver share the same optical axis and are located at the same distance from the cloud. The source is a nominal 1-W, 1.06- $\mu$ m wavelength and 100-mm diameter collimated laser beam. The receiver has an aperture of 250 mm and an adjustable field of view. The range-resolved lidar backscattered power  $P(R)$  is calculated per unit length so that the power received from range  $R$  for a pulsed laser of average pulse power  $P_0$  in watts and pulse duration  $\tau$  is given by  $P_0 P(R) c \tau / 2$ , where  $c$  is the speed of light and  $c \tau$  is expressed in km. For example, Fig. 5 shows the lidar signals  $P(R)$  obtained from the cloud defined in Fig. 3 for a cloud-to-receiver distance of 1 km and fields of view (half angle) of 1, 20, 50 and 100 mrad. The lidar returns increase with field of view because of multiscattering contributions.

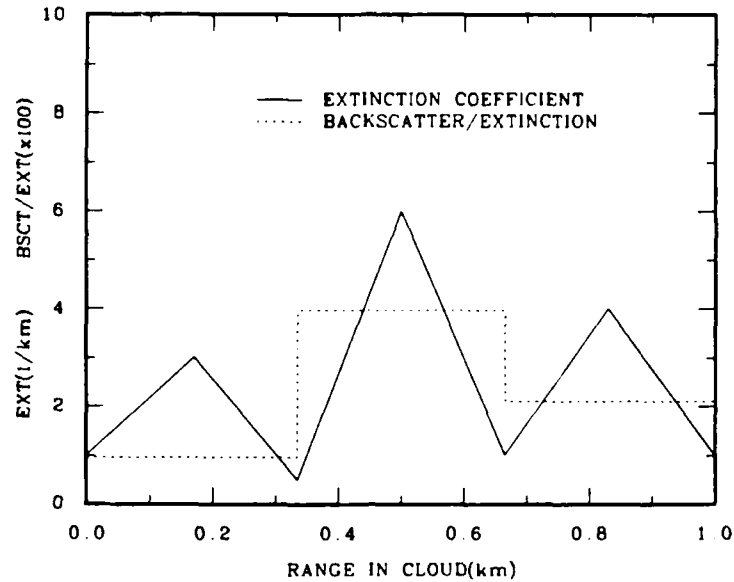


FIGURE 3 - Same as Fig. 1 but for a cloud made up of three regions consisting of urban, maritime and rural aerosols at 70% relative humidity (Ref. 11), respectively.

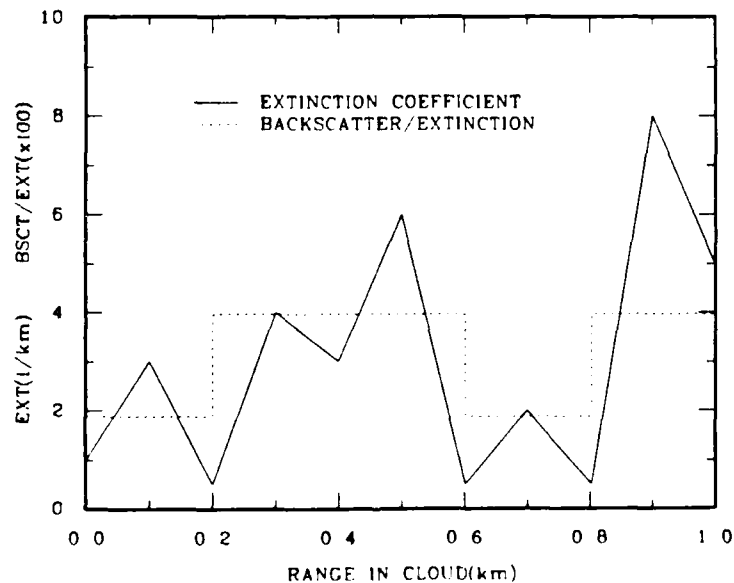


FIGURE 4 - Same as Fig. 1 but for a cloud made up of the alternate juxtaposition of the generic rural aerosol model at 99% relative humidity and the maritime model at 70% relative humidity (Ref. 11), respectively.

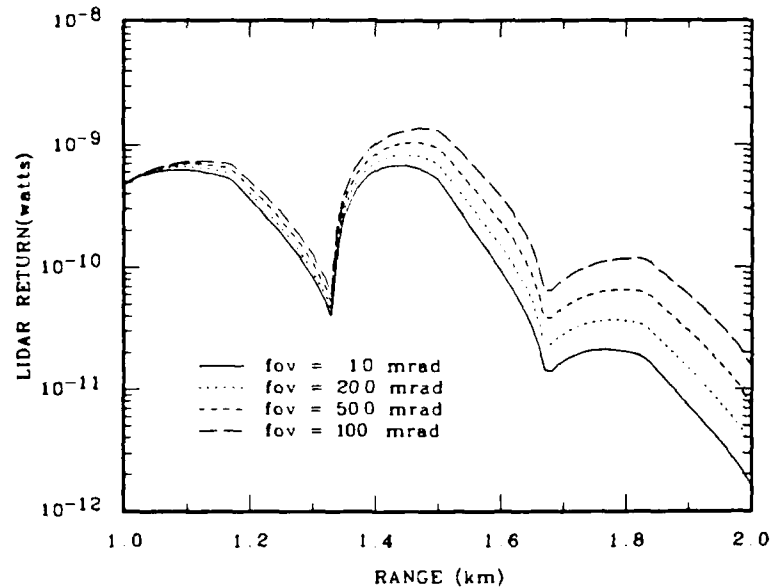


FIGURE 5 - Example of calculated lidar signals at receiver fields of view (half angle) of 1, 20, 50 and 100 mrad for the cloud defined in Fig. 3 and for a cloud-to-receiver distance of 1 km. The source is a 1-W, 1.06- $\mu$ m and 100-mm diameter collimated laser beam and the receiver aperture diameter is 250 mm. The calculations were performed with the propagation model of Ref. 10.

### 3.0 SINGLE-SCATTERING LIDAR INVERSION

#### 3.1 Solution Methods

Although the object of this report is to introduce a new lidar inversion algorithm based on recovering the information contained in the multiscattering contributions, it is important to compare results with solutions derived from the well-known single-scattering lidar equation. The single-scattering lidar solution methods are reviewed briefly and the calculation results for the clouds defined in Figs. 1-4 are presented and discussed.

According to the single-scattering theory, the range-resolved lidar backscattered power per unit length is given by

$$P_s(R) = P_o \frac{A}{R^2} \beta(R) \exp \left\{ -2 \int_0^R \alpha_e(r) dr \right\}, \quad [1]$$

where  $P_o$  is the transmitter power,  $A$  is the area of the receiver aperture,  $R$  is the range,  $\beta$  is the backscatter coefficient, and  $\alpha_e$  is the extinction coefficient. A more convenient signal variable is the logarithmic range-adjusted power defined as

$$S(R) = \ln \left[ \frac{R^2 P_s(R)}{R_m^2 P_m} \right], \quad [2]$$

where  $R_m$  and  $P_m$  are unspecified normalization constants. In terms of  $S(R)$ , eq. 1 can be rewritten in the following differential form:

$$\frac{dS}{dR} = \frac{1}{\beta} \frac{d\beta}{dR} - 2 \alpha_e. \quad [3]$$

Equation 3 relates one measured function  $S(R)$  to two unknown functions  $\beta(R)$  and  $\alpha_e(R)$ . To solve  $\alpha_e$ , a functional relationship must be given or assumed between  $\beta$  and  $\alpha_e$ . The most common assumption is to postulate that

$$\beta(R) = C(R) \alpha_e^k(R), \quad [4]$$

where  $k$  is constant. The function  $C(R)$  is unknown a priori.

The solution of the first-order differential eq. 3 necessitates the specification of one boundary value. To keep the solution as general as possible, we assume that the extinction coefficient is known or given at some arbitrary range  $R_f$ , i.e.  $\alpha_f = \alpha_e(R_f)$ . After substitution of eq. 4 for  $\beta(R)$ , the solution of eq. 3 (Ref. 2) is then given by

$$\alpha_e(R) = \frac{\left[ \frac{C(R_f)}{C(R)} \right]^{1/k} \exp \left[ \frac{S(R) - S(R_f)}{k} \right]}{\alpha_f^{-1} - \frac{2}{k} \int_{R_f}^R \left[ \frac{C(R_f)}{C(r)} \right]^{1/k} \exp \left[ \frac{S(r) - S(R_f)}{k} \right] dr} . \quad [5]$$

Equation 5 contains the function  $C(R)$ . In general, we cannot expect to know  $C(R)$  until  $\alpha_e(R)$  is determined.  $C(R)$  is, in fact, part of the solution and  $\alpha_e(R)$  cannot be solved for unless independent information, in addition to  $S(R)$ , is given. This constitutes one major difficulty for the solution of the single-scattering lidar equation. One convenient simplification consists in assuming that  $C(R) = \text{cst.}$  As shown by eq. 5, the solution for  $\alpha_e(R)$  then becomes independent of the value of  $C$ . This approximation is truly valid only if the composition, geometry and size distribution of the aerosol particles are invariant.

It is emphasized that the boundary value  $\alpha_f$  cannot be arbitrary. The apparent one-constant arbitrariness associated with the first-order derivative of eq. 3 is not a property of the physical problem since the differentiation was carried out for convenience only. The physical process measured by the function  $S(R)$  is actually modeled by eq. 1 which involves no derivatives. Hence, the boundary value  $\alpha_f$  must be consistent with  $S(R)$ .

Originally, eq. 5 was used with the boundary value specified at the near-end boundary of the cloud, i.e. at  $R_f < R$ . The obvious advantage is that the extinction coefficient  $\alpha_f$  is easier to measure or estimate at close range than at far range. However, calculation results (Ref. 1) and a theoretical analysis (Ref. 5) have shown that the solution given by eq. 5 is unstable if  $R_f < R$ . Small errors cause the solution to vanish or grow indefinitely. By contrast, the same analyses (Refs. 1 and 5) have demonstrated that the solution of eq. 5 is stable if  $\alpha_f$  is specified at the far-end boundary or backside of the

cloud, i.e.  $R_f > R$ . The problem, however, is to obtain a reasonable estimate of  $\alpha_f$ . This constitutes a second major difficulty affecting the inversion of the single-scattering lidar equation.

### 3.2 Results

To illustrate the stability problem, we have applied the solution of eq. 5 to the lidar signal generated for the cloud defined in Fig. 1. In this report, we make the parameter  $k$  of eqs. 4 and 5 equal to unity. Since  $C(R)$  is allowed to vary, this condition has no incidence on the generality of the solutions. For the conditions of Fig. 1, we have  $C(R) = 0.038 = \text{cst}$  and eq. 5 can be used with no further approximation to calculate  $\alpha_e(R)$ . The 1-mrad field-of-view (half angle) signal  $S(R)$  is used for this application. This field of view is sufficiently small to minimize the multiscattering contributions and it simulates well practical applications.

Figure 6 compares the true profile of the extinction coefficient with the solutions obtained by specifying the value of  $\alpha_f$  at the near-end boundary of the cloud. Three solutions were calculated for  $\alpha_f = 0.9, 1.0$  and  $1.1 \text{ km}^{-1}$  respectively, the true value being  $1.0 \text{ km}^{-1}$ . As shown, the solutions for  $\alpha_f = 1.0$  and  $1.1 \text{ km}^{-1}$  diverge to infinity while that for  $\alpha_f = 0.9 \text{ km}^{-1}$  quickly falls off to zero. Even the solution for the true  $\alpha_f$  value of  $1.0 \text{ km}^{-1}$  diverges because the 1-mrad simulated lidar signal contains enough multiscattering contributions to cause irrecoverable instability. Therefore, Fig. 6 shows that the solutions based on the near-end boundary condition are totally deficient and unacceptable for conditions represented by the cloud defined in Fig. 1. By comparison, Fig. 7 shows the solutions for the same values of  $\alpha_f$  but specified at the far-end boundary of the cloud where the true  $\alpha_e$  is also  $1.0 \text{ km}^{-1}$ . All three solutions are acceptable; the original errors in  $\alpha_f$  are damped and the three curves converge to a

single one as the front end of the cloud is approached. The small differences with the true profile come from the multiscattering contributions which are not taken into account by the single-scattering lidar equation. In summary, the results illustrated in Figs. 6 and 7 only confirm previous findings (Refs. 1 and 5) that the stability of the single-scattering lidar equation requires that the boundary condition be given or specified at the far end of the lidar range where the signal  $S(R)$  is generally smallest.

Figure 8 shows the solutions obtained for the same cloud and with the same method as in Fig. 7 but given large errors in  $\alpha_f$ , namely  $\alpha_f = 0.1$  and  $3.0 \text{ km}^{-1}$  compared with the true value of  $1.0 \text{ km}^{-1}$ . The solutions eventually converge as expected, but the errors remain large over a nonnegligible portion of the cloud. This is especially true in the case of  $\alpha_f = 0.1 \text{ km}^{-1}$  where the differences normalized to the cloud average extinction coefficient of  $3.5 \text{ km}^{-1}$  can grow as high as 80% before being damped. Therefore, a reasonable estimate of  $\alpha_f$  on the far side of the cloud is an important requirement even though large errors do not cause irrecoverable instabilities. Good accuracy in estimating or independently measuring  $\alpha_f$  is difficult to achieve since the far-side boundary is shielded from the lidar station by the cloud itself. For clouds of arbitrary extinction profiles, there is yet no systematic method of deriving  $\alpha_f$  from lidar data.

The example of Fig. 8 as well as many other calculations show that the solutions converge more rapidly if  $\alpha_f$  is overestimated rather than underestimated. For instance, the solution based on  $\alpha_f = 3.0 \text{ km}^{-1}$  becomes acceptable at about the 2/3 point of the cloud (measured from the front end), while this occurs only at the 1/3 mark for the solution based on  $\alpha_f = 0.1 \text{ km}^{-1}$ . This is in agreement with the theoretical analysis of Ref. 5 (eq. 15) which shows that the relative error on the calculated extinction coefficient is inversely proportional to the boundary value.

As discussed earlier, a fundamental characteristic of the single-scattering lidar inversion problem described by eqs. 1-5 is that a relation between the extinction and backscattering coefficients must be assumed. We have seen that the simplification  $C(R) = \text{cst}$  can be made if the composition, geometry and size distribution of the aerosol particles remain invariant. We will now investigate if this simplification can be applied to more realistic clouds of variable  $C(R)$ . The cloud defined in Fig. 2 has the same extinction profile as in Fig. 1 but it differs by a smoothly varying function  $C(R)$ . The solutions obtained for this cloud under the assumption of a constant  $C(R)$  are plotted in Fig. 9. The boundary values are as in Fig. 8, i.e.  $\alpha_f = 0.1, 1.0$  and  $3.0 \text{ km}^{-1}$  specified at the far-end boundary of the cloud. The solutions are not very much different from those of Fig. 8 for a truly constant  $C(R)$ . They tend to be greater in regions where  $C(R)$  is greater than its value at the boundary point and vice versa, which is in agreement with the analytic expressions (eqs. 12 and 15) derived in Ref. 5. The symmetry of the calculated extinction distribution is thus skewed, even for the exact boundary value. However, the largest errors are again associated with the boundary-value errors.

The solutions for the more complex case of Fig. 3, where regions of constant but different  $C(R) = \beta/\alpha_e$  are juxtaposed, are shown in Fig. 10. For the exact  $\alpha_f$ , the solution remains exact so long as  $C(R)$  does not change from its value at the far-end boundary. With the step changes in  $C(R)$ , the computed extinction coefficient becomes in error by an amount that appears to be proportional to the magnitude of the step. If  $C(R)$  increases, the extinction coefficient becomes greater than the true value and vice versa. For the conditions of Fig. 10, the differences resulting from the assumption of constant  $C(R)$  can become as high as  $2/3$  times the local true extinction coefficient. It is emphasized, however, that nowhere in Figs. 9 and 10, nor in other calculations, did the assumption of constant  $C(R)$  lead to catastrophic results as in Fig. 6 for the near-end solution.

The solutions for the clouds defined in Figs. 2 and 3 were recalculated after substitution in eq. 5 of their respective true function  $C(R)$ . The results are plotted in Figs. 11 and 12 respectively. The solutions for the true  $\alpha_f$  boundary value reproduce almost exactly the true extinction profiles. The solutions for the erroneous  $\alpha_f$  remain in error in the far-end region of the cloud but gradually tend toward the true profile with decreasing range. As previously noted, the errors are less if the boundary value is overestimated. Finally, it can be observed that the solutions of Fig. 11 are very close to those of Fig. 8; the true extinction profiles are indeed the same in both cases, only the functions  $C(R)$  are different. This result confirms that the single-scattering lidar solution gives the correct extinction coefficient if  $C(R)$  is known.

The solutions of Figs. 11 and 12 show that the knowledge of  $C(R)$  allows the determination of the extinction coefficient profile with a precision dictated only by that of its boundary value at the far side of the cloud and, of course, by the experimental errors. However, they give no clue as to how this input can be obtained in practice. The lidar signal alone is not sufficient. Additional information on the nature of the aerosol particles is required, for example in the form of an empirical correlation between  $\beta$  and  $\alpha_e$  as suggested by Klett (Ref. 2).

The solutions of Figs. 8 and 11 calculated with the exact boundary value and the prescribed  $C(R)$  functions differ slightly although the true extinction profile is the same in both cases. The reason is multiscattering contributions. These contributions are more important in the case of Fig. 8 because the forward-scattering peak is narrower for the 99% relative humidity maritime aerosol (Fig. 8) than for the mixture of rural, urban and maritime aerosols at 70% relative humidity (Fig. 11). Indeed, a narrower forward peak means that more forward-scattered radiation remains in the receiver field of view. As

illustrated in Figs. 8 and 11, the multiscattering contributions have the effect of reducing the extinction coefficient calculated with the single-scattering lidar equation. This is easily understood from eq. 1. The increase of the lidar signal by multiscattering returns is interpreted by eq. 1 as a drop in the extinction coefficient since the exponential is a faster function than the linear backscatter term (proportional to  $\alpha_e^k$  according to eq. 4).

The multiscattering effect depends on several factors. First, there is the nature of the aerosols which explains, as we have just seen, the differences between Figs. 8 and 11. The important property is the width of the forward scattering peak; the narrower the width, the greater the probability of recording multiscattering contributions by a receiver of given field of view. Second, there is the cloud optical depth. For a given aerosol, the multiscattering returns increase with the optical depth. For example, Fig. 13 shows what happens if the aerosol concentration of the cloud defined in Fig. 1 is doubled. Comparing the results depicted in Figs. 8 and 13, we observe that the single-scattering solution underestimates substantially the extinction coefficient at greater optical depths. Finally, an obvious factor is the receiver field of view. Figure 14 contrasts the solutions derived from lidar signals obtained from the same cloud with receiver fields of view of 1, 5 and 20 mrad. The predicted extinction coefficient decreases with widening field of view, which is in agreement with the preceding observations on the effect of increasing multiscattering contributions. In practice, different cloud-to-receiver distances will produce the same result. This is illustrated in Fig. 15 where the solutions for the 1-mrad lidar signals are presented for cloud-to-receiver distances of 0.2, 1.0 and 3.0 km.

Based on the preceding results, the following observations can be made on the use of the single-scattering lidar equation to determine the aerosol extinction coefficient:

- a) At extinction coefficients of the order of  $1 \text{ km}^{-1}$  or greater, the near-end boundary value inversion algorithm is unstable to small errors in the assumed boundary value and to small, but unavoidable, multiscattering contributions. The same is probably true for experimental errors. The instabilities are irrecoverable and make the method useless in most applications involving clouds.
- b) The far-end boundary value inversion algorithm is stable to any perturbations resulting from boundary value errors, uncertainties in the backscatter-to-extinction ratio, and/or multiscattering contributions. The remaining comments concern solutions obtained with this method.
- c) It is the boundary value errors that most affect the calculated extinction coefficient. Although the solutions eventually converge to the true profiles, the convergence rate depends on the initial gap, and the residual errors may be large. For all cases studied, the convergence rate is faster if the assumed far-end extinction coefficient is overestimated. The determination of the boundary value is a serious problem, and the information contained in the single-scattering lidar signal is not sufficient to permit a reliable estimate for arbitrary extinction profiles.
- d) The errors resulting from the assumption of a constant profile of the backscatter-to-extinction ratio  $\beta/\alpha_e$  are, surprisingly, within acceptable limits. For step changes in  $\beta/\alpha_e$  of the order of 4, errors in the local extinction coefficient may exceed 100%, but the general shape of the profile is obtained and the average aerosol extinction coefficient over the cloud depth is within 10-20% of the true value. If the function  $\beta/\alpha_e$  is known, the solution

converges to the true extinction profile. For practical applications, additional and independent information on the nature of the aerosol particles is required to determine or estimate  $\beta/\alpha_e$ .

- e) If the receiver field of view is chosen to stare only at the volume probed by the unscattered transmitter beam and if that beam is reasonably collimated, the solution errors caused by multiscattering contributions remain below a few percent up to an optical depth between 3 and 4. The degradation beyond this limit is quite rapid, but it is questionable whether lidar measurements remain reliable for optical depths greater than 3-4.

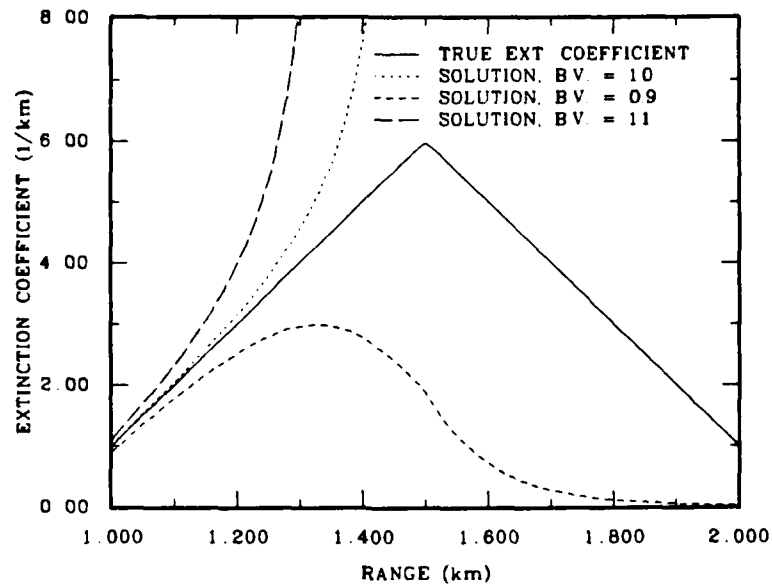


FIGURE 6 - Single-scattering lidar solutions for the cloud defined in Fig. 1 calculated with the near-end boundary value algorithm. The solutions were obtained with extinction coefficient boundary values (B.V.) of 0.9, 1.0 and 1.1  $\text{km}^{-1}$  for a true value of 1.0  $\text{km}^{-1}$ .

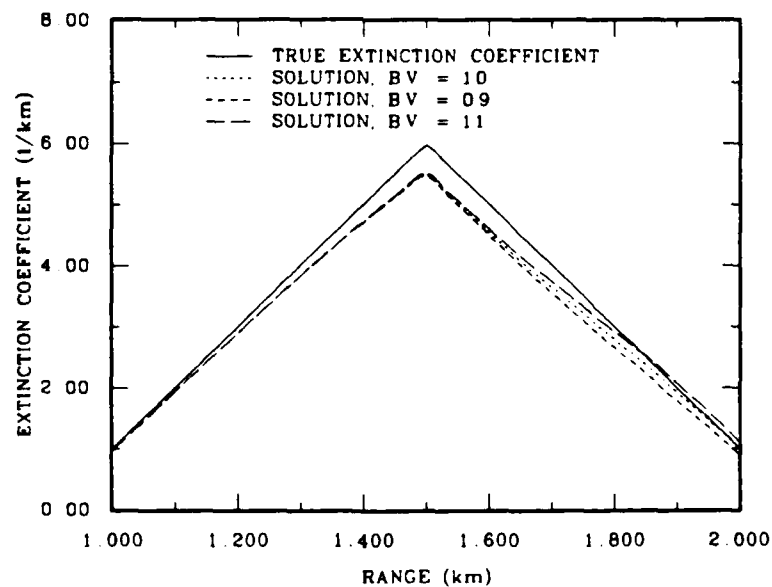


FIGURE 7 - Single-scattering lidar solutions for the cloud defined in Fig. 1 calculated with the far-end boundary value algorithm. The solutions were obtained with extinction coefficient boundary values (B.V.) of 0.9, 1.0 and 1.1  $\text{km}^{-1}$  for a true value of 1.0  $\text{km}^{-1}$ .

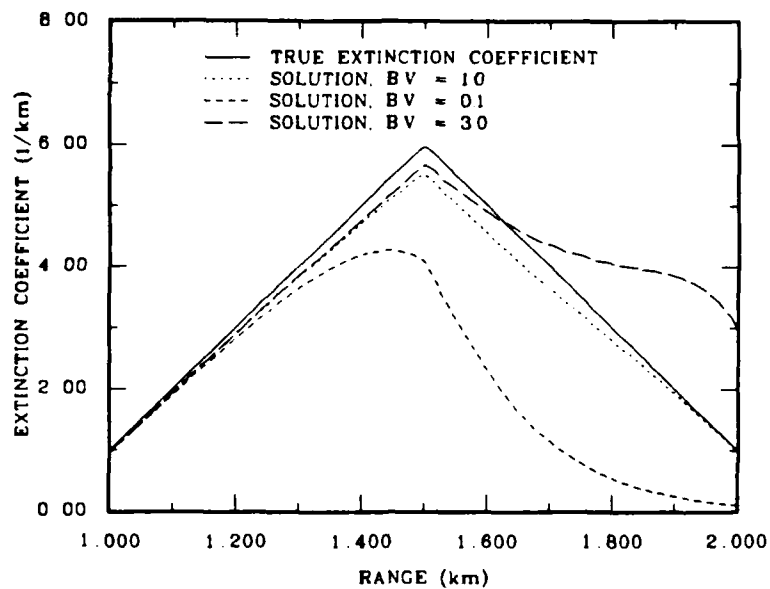


FIGURE 8 - Same as Fig. 7 but for boundary values (B.V.) of 0.1, 1.0 and 3.0  $\text{km}^{-1}$ .

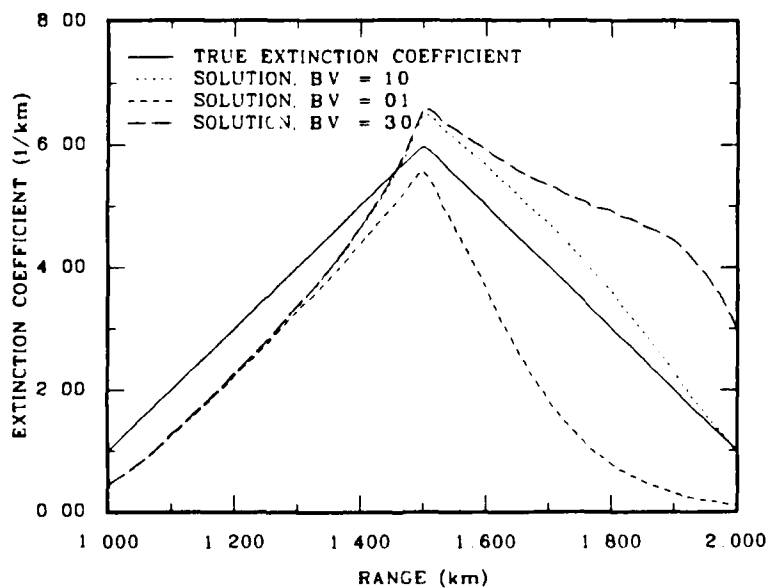


FIGURE 9 - Single-scattering lidar solutions for the cloud defined in Fig. 2 calculated with the far-end boundary value algorithm. The solutions were obtained under the assumption of a constant  $\beta/\alpha_e$  ratio with boundary values (B.V.) of 0.1, 1.0 and 3.0  $\text{km}^{-1}$  for a true value of 1.0  $\text{km}^{-1}$ .

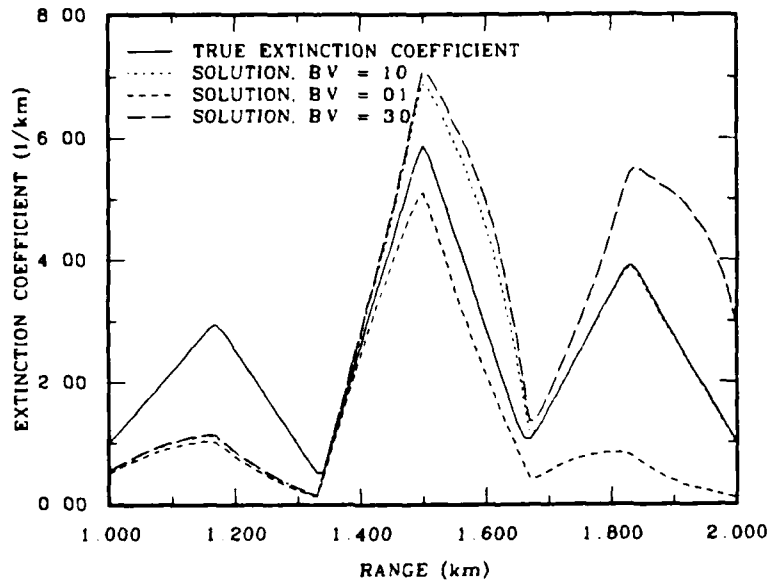


FIGURE 10 - Same as Fig. 9 but for the cloud defined in Fig. 3.

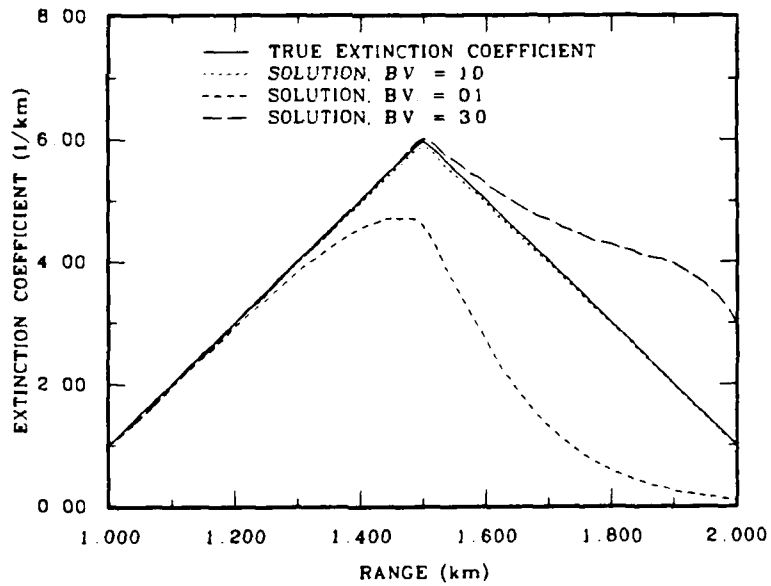


FIGURE 11 - Same as Fig. 9 except that the solutions were calculated with the true  $\beta/\alpha_e$  profile.

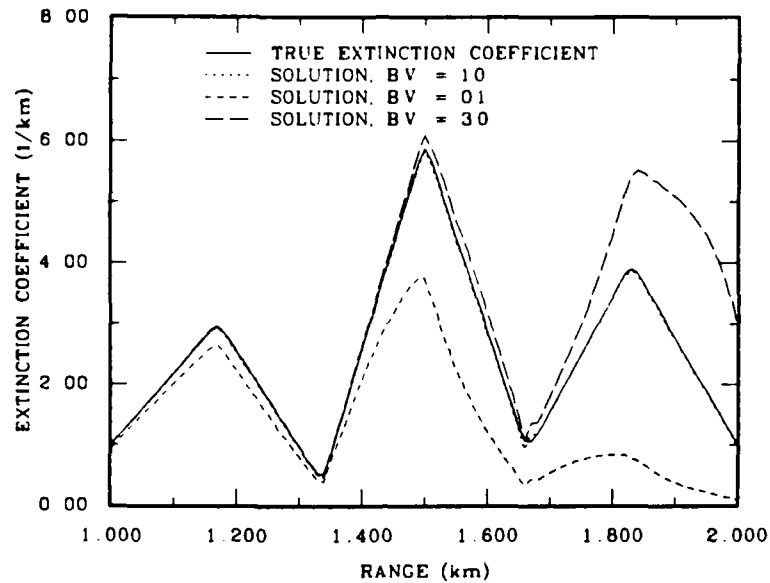


FIGURE 12 - Same as Fig. 10 except that the solutions were calculated with the true  $\beta/\alpha_e$  profile.

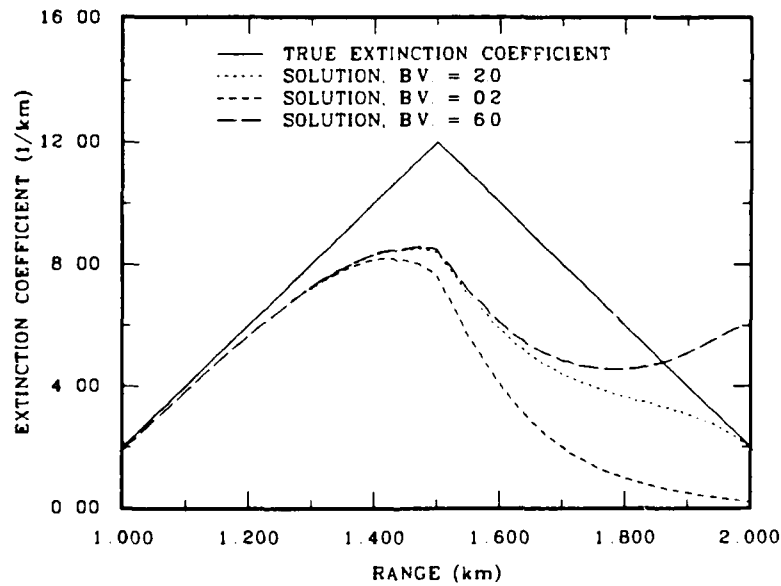


FIGURE 13 - Single-scattering lidar solutions calculated with the far-end boundary value algorithm for the cloud defined in Fig. 1 except that the extinction profile was doubled to exemplify the multiscattering effects. The solutions were obtained with boundary values (B.V.) of 0.2, 2.0 and 6.0  $\text{km}^{-1}$  for a true value of 2.0  $\text{km}^{-1}$ .

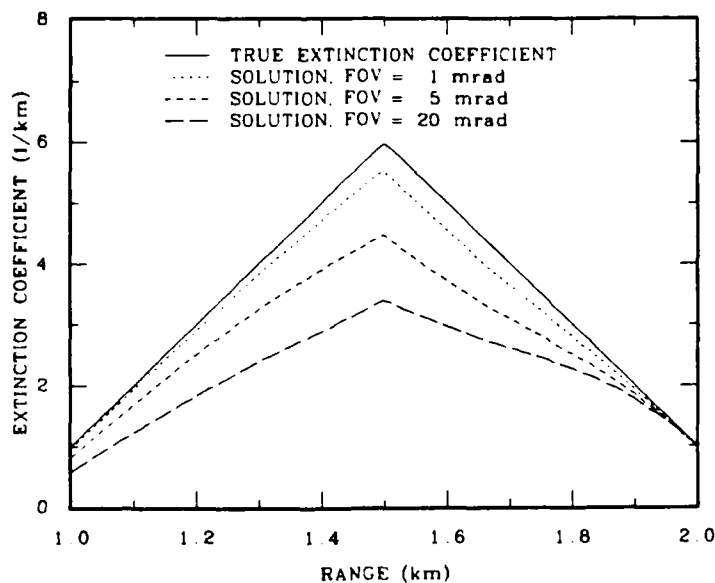


FIGURE 14 - Single-scattering lidar solutions calculated with the far-end boundary value algorithm for the lidar signals from the cloud defined in Fig. 1 generated with fields of view (FOV) of 1, 5 and 20 mrad. The true boundary value of  $1.0 \text{ km}^{-1}$  was used for all three solutions.

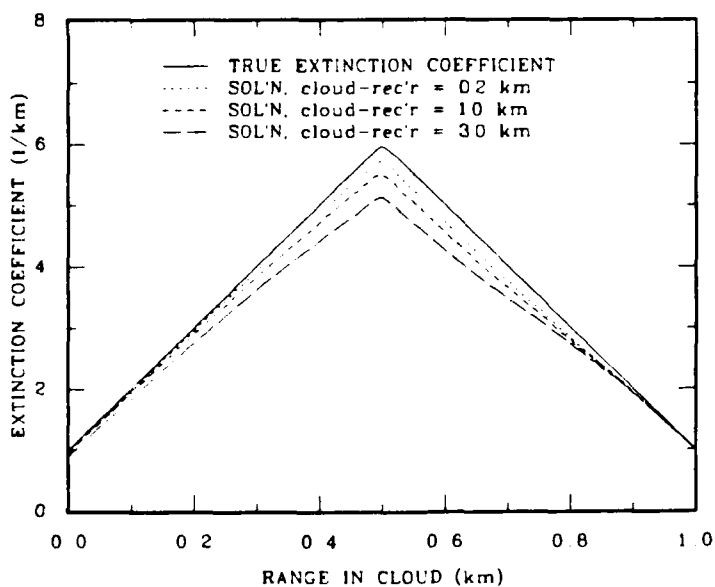


FIGURE 15 - Single-scattering lidar solutions calculated with the far-end boundary value algorithm for the lidar signals from the cloud defined in Fig. 1 generated with a field of view of 1 mrad but cloud-to-receiver distances (cloud-rec'r) of 0.2, 1.0 and 3.0 km. The true boundary value of  $1.0 \text{ km}^{-1}$  was used for all solutions.

4.0 MULTISCATTERING INVERSION METHOD4.1 Solution Method

The proposed lidar solution method is derived from the multi-scattering propagation model described in Ref. 10. The aim is to make use of the information carried by the higher order scattering events occurring on both transmission legs to and from the probed volume. From the solution of Ref. 10 for the backscattered radiant intensity, the power detected by a lidar receiver that shares the same axis as the transmitter is given by

$$P(R, \omega) = \frac{P_o A}{\pi \omega_o^2} \alpha_s^-(R) \exp\left[-2 \int_0^R (\alpha_m + \alpha_a + \alpha_s^-) dr\right] \\ \times \left\{ \frac{U(R, \omega)}{K(R)} \exp\left[-\int_0^R \alpha_s^+ dr\right] + V(R, \omega) \int_0^R \frac{dr'}{M(R, r')} \alpha_s^+(r') \exp\left[-\int_0^{r'} \alpha_s^+ dr\right] \right\} \quad [6]$$

where  $P_o$  is the transmitter power,  $\omega_o$  is the zero-range radius of the transmitter beam,  $A$  is the collecting area of the receiver,  $R$  is the range,  $\omega$  is the receiver field of view, and  $\alpha_m$  is the molecular absorption coefficient. The aerosol scattering and absorption properties are given by the backscattering coefficient

$$\alpha_s^- = \int_{\pi/2}^{\pi} d\theta \sin\theta \int_0^{2\pi} d\phi \int_0^{\infty} d\rho \frac{dN(\rho)}{d\rho} \pi \rho^2 \frac{dQ_s}{d\Omega}(\theta, \phi, \rho), \quad [7]$$

the forward scattering coefficient

$$\alpha_s^+ = \int_0^{\pi/2} d\theta \sin\theta \int_0^{2\pi} d\phi \int_0^{\infty} d\rho \frac{dN(\rho)}{d\rho} \pi \rho^2 \frac{dQ_s}{d\Omega}(\theta, \phi, \rho), \quad [8]$$

and the aerosol absorption coefficient

$$\alpha_a = \int_0^\infty d\rho \frac{dN(\rho)}{d\rho} \pi \rho^2 Q_e(\rho) - (\alpha_s + \alpha_s^-), \quad [9]$$

where the angles  $\theta$  and  $\phi$  define the scattering direction,  $\rho$  is the particle radius,  $dN/d\rho$  is the particle size probability density,  $dQ_s/d\Omega$  and  $Q_e$  are the differential scattering and total extinction efficiencies of a particle of size  $\rho$ , and  $d\Omega$  is the differential solid angle. The functions  $K(R)$  and  $M(R, r')$  are broadening functions for the forward- and backscattered beams respectively. If the transmitter beam is collimated within a few mrad,  $K(R)$  and  $M(R, r')$  are given by

$$K(R) = 1 + \frac{4}{w_0^2} \int_0^R D^-(R, r) dr, \quad [10]$$

$$M(R, r') = 1 + \frac{4}{w_0^2} \int_0^R D^-(R, r) dr + \frac{4}{w_0^2} \int_{r'}^R D^+(r', r) dr, \quad [11]$$

where  $D^+$  and  $D^-$  are lateral diffusion coefficients defined by

$$D^+(r', r) = (r - r') \frac{\int_0^{\pi/2} d\theta \sin\theta p(\theta)}{\int_0^{\pi/2} d\theta p(\theta)}, \quad [12]$$

$$D^-(R, r) = (R - r) \frac{\int_0^\pi d\theta \sin\theta p(\theta)}{p(\pi)}. \quad [13]$$

In eqs. 12 and 13,  $p(\theta)$  is the aerosol scattering phase function assumed to be rotationally symmetric.

The remaining functions  $U(R, \omega)$  and  $V(R, \omega)$  are field-of-view reduction factors given in Ref. 10. They depend on  $\omega$  and the scattering properties of the aerosols. They are complicated functions of these arguments but only their asymptotic values will be used here.

For optical and infrared lidar applications in the atmosphere, the scattering phase function  $p(\theta)$  is much more sharply peaked in the forward than in the backward direction. It follows from eqs. 12 and 13 that  $D^+/(r-r') \ll D^-(R-r')$  and we can neglect the third term on the right-hand side of eq. 11. Hence,

$$M(R, r') \approx K(R), \quad [14]$$

and eq. 6 becomes

$$P(R, \omega) = \frac{P_o A}{\pi \omega_o^2 K(R)} \alpha_s^-(R) \exp\left[-2 \int_0^R (\alpha_m + \alpha_a + \alpha_s^-) dr\right] \\ \times \left\{ U(R, \omega) \exp\left[-\int_0^R \alpha_s^+ dr\right] + V(R, \omega) \left[1 - \exp\left(-\int_0^R \alpha_s^+ dr\right)\right] \right\}. \quad [15]$$

Equation 15 is the proposed modified lidar equation that takes into account multiple scatterings. It is instructive to consider two asymptotic forms of eq. 15. First, we examine the case of an open receiver, i.e. a field of view (half angle)  $\omega$  equal to  $\pi/2$ . By definition (Ref. 10),  $U$  and  $V$  tend to unity in that limit and eq. 15 becomes

$$P(R, \pi/2) = \frac{P_o A}{\pi \omega_o^2 K(R)} \alpha_s^-(R) \exp\left[-2 \int_0^R (\alpha_m + \alpha_a + \alpha_s^-) dr\right]. \quad [16]$$

Second, we consider the situation where the receiver field of view stares at the volume probed by the unscattered transmitter beam only. In other words, the field of view is chosen equal or just slightly greater than the transmitter beam divergence assumed to be small. For that condition, it can be shown from the expressions of Ref. 10 for  $U$  and  $V$  that

$$\lim_{\omega \rightarrow \omega_t} V(R, \omega) \approx 0, \quad [17]$$

$$\lim_{\omega \rightarrow \omega_t} U(R, \omega) = \exp\left[- \int_0^R \alpha_s^+ dr\right], \quad [18]$$

where  $\omega_t$  is equal to the transmitter divergence. Physically, eqs. 17 and 18 state that multiscattering contributions are not significant at such small fields of view: the fraction  $V$  of the multiscatter signal that would originate from the forward-scattered beam is approximately zero since the receiver field of view sees only a small region of that broadened beam, and the fraction  $U$  arising from the unscattered beam falls off as  $\exp\left[- \int_0^R \alpha_s^+ dr\right]$  since the radiation scattered on the transmission path back to the receiver is collected in a negligible amount because of the small field of view. The approximations of eqs. 17 and 18 begin to fail at optical scattering depths  $\int_0^R \alpha_s^+ dr$  beyond 3-4. Substituting eqs. 17 and 18 for  $U$  and  $V$  in eq. 15, we obtain

$$P(R, \omega_t) = \frac{P_o A}{\pi \omega_o^2 K(R)} \alpha_s^-(R) \exp\left[- 2 \int_0^R (\alpha_m + \alpha_a + \alpha_s^- + \alpha_s^+) dr\right]. \quad [19]$$

Except for slight differences in the formulations of the backscatter coefficient  $\alpha_s^-$  and geometric factor  $K(R)$ , eq. 19 is similar to the single-scattering lidar equation. Both give approximately the same answers for  $P$  as demonstrated by the results of Ref. 10.

If we ratio eqs. 16 and 19, we obtain

$$\frac{P(R, \pi/2)}{P(R, \omega_t)} = \exp\left[2 \int_0^R \alpha_s^+ dz\right]. \quad [20]$$

Equation 20 is at the origin of the proposed multiscattering lidar inversion method. If we could record simultaneously the lidar returns at both fields of view  $\omega_t$  and  $\pi/2$ , we could easily determine the

forward-scattering coefficient  $\alpha_s^+$  from eq. 20. The technique would require no instrument calibration, no relationship between backscatter and extinction, and no boundary value. It could thus be free of the most serious difficulties associated with the solution of the single-scattering lidar equation. The parameter determined would be the forward-scattering coefficient which is, within a few percent, equal to the albedo times the extinction coefficient.

The technique suggested by eq. 20 is straightforward, but lidar measurements at wide fields of view, as required for  $P(R, \pi/2)$ , are not practical because of signal-to-noise problems. Nonetheless, the ratioing principle can still be applied to simultaneous measurements at smaller fields of view and still carry the advantages of no requirements for a boundary value and for a backscatter-to-extinction relation. Equation 20 would have to be replaced by an expression involving the functions  $U$  and  $V$ . Since  $U$  and  $V$  are complicated functions of their arguments, they do not provide, in general, a mathematical form useful for inversion algorithms. However, calculation results and the asymptotic form of eq. 20 suggest the following simple empirical formula:

$$\frac{d}{dR} \ln \left[ \frac{P(R, \omega)}{P(R, \omega_t)} \right] = 2 f(\omega, \omega_t) \alpha_s^+(R), \quad [21]$$

where  $\omega$  is a receiver field of view greater than  $\omega_t$ , and  $f(\omega, \omega_t)$  is a function of  $\omega$  and  $\omega_t$  to be determined empirically.  $f(\omega, \omega_t)$  is not a universal function, it depends on the aerosol properties.

By definition,  $\omega_t$  is small and approximately equal to the transmitter beam divergence. On the other hand, the field of view  $\omega$  must be chosen large enough to make  $f(\omega, \omega_t)$  measurable but as small as possible to minimize the noise problems. Calculation results obtained under these conditions suggest the following empirical form:

$$f(\omega, \omega_t) = (\chi/b)^k, \quad [22]$$

with

$$\chi = \ln \left\{ \frac{\sqrt{W_o} + \sqrt{\omega R}}{\sqrt{W_o} + \sqrt{\omega_t R}} \right\}, \quad [23]$$

for  $\omega_t < \omega \ll \pi/2$ , where  $W_o$  is the radius of the receiver aperture. The parameter  $b$  appears to be a system constant, but  $k$  depends on the aerosol properties and can vary with range  $R$ . Figure 16 shows how eq. 22 compares with calculated lidar signals for two types of aerosols. The power law function provides a very good fit up to fields of view (half angle) of the order of 100 mrad. The aerosols chosen represent conditions that are as far apart as possible for the AFGL generic models at the 1.06- $\mu$ m wavelength. The backscatter-to-extinction ratio and albedo are 0.038 and 0.998, and 0.010 and 0.634 for the maritime and urban aerosols used for the calculations illustrated in Fig. 16, respectively. Calculations with different clouds produced similar fits with local discrepancies less than 5% for fields of view (half angle) smaller than about 100 mrad. The empirical model defined by eqs. 22-23 constitutes one convenient choice but some other functional dependence could probably give similar or even better results.

Equations 21-23 form the basis of a very simple lidar inversion technique. If the lidar return is recorded simultaneously at three fields of view  $\omega_t$ ,  $\omega_1$  and  $\omega_2$ , the exponent  $k$  can be calculated with the formula

$$k(R) = \frac{\ln \left\{ \frac{d}{dR} \ln[P(R, \omega_1)/P(R, \omega_t)] / \frac{d}{dR} \ln[P(R, \omega_2)/P(R, \omega_t)] \right\}}{\ln[\chi_1/\chi_2]}, \quad [24]$$

where  $\chi_1$  and  $\chi_2$  are obtained by substitution of  $\omega_1$  and  $\omega_2$  for  $\omega$  in eq. 23. In practice, the ratios  $P(R, \omega_1)/P(R, \omega_t)$  and  $P(R, \omega_2)/P(R, \omega_t)$

should be smoothed to minimize the fluctuations resulting from the finite difference approximations to the derivatives of eq. 24.

Once  $k(R)$  is determined, the forward-scattering coefficient  $\alpha_s^+$  is calculated with the following formula derived from eq. 21:

$$\alpha_s^+(R) = \frac{1}{2} (b/\chi)^k \frac{d}{dR} \ln[P(R, \omega)/P(R, \omega_t)], \quad [25]$$

for  $\omega = \omega_1$  and/or  $\omega_2$ , and  $\chi$  is given by eq. 23. The parameter  $b$  is a system constant and must be determined by calibration or other means. The results plotted in Fig. 16 show that different aerosols give different exponents  $k$ . Since  $k$  is computed at each range  $R$ , the method is therefore applicable to clouds of varying composition.

Equations 24 and 25 define the proposed multiscattering lidar inversion algorithm. It is based on the simultaneous measurement of the lidar returns at three fields of view. One field of view must be chosen equal to or just slightly above the transmitter divergence. The other two are greater but just enough to give measurable differences. Since only ratios are used in the algorithm, no individual signal calibration is necessary. The ratios are simply adjusted to tend to unity at the front end of the cloud or zero optical depth. The solution for the forward scattering coefficient  $\alpha_s^+$  is calculated by straightforward substitution in the algebraic formulas 23-25. No backscatter-to-extinction relation and no boundary value are required. Equation 25 shows that the proposed inversion method is very similar to the simple slope method but applied to the lidar ratio  $P(R, \omega)/P(R, \omega_t)$ .

#### 4.2 Results

The proposed multiscattering lidar inversion technique is applied to the signals generated for the clouds defined in Figs. 1-4. Examples of lidar ratios used for the calculations are shown in Fig. 17, they were obtained for the cloud profiles of Fig. 3. These results illustrate the magnitude of the signal differences that can be expected in atmospheric-like aerosols for fields of view (half angle) of 1, 20, 50 and 100 mrad. Such differences are measurable with acceptable signal-to-noise ratios. Near simultaneous measurements of lidar returns at 1 and 3 mrad off marine stratus clouds with a 480-m altitude cloud base (Ref.6) showed a signal ratio that can reach a value of 2. Therefore, the calculated ratios of order 10 or less plotted in Fig. 17 appear reasonable considering the greater differences in fields of view.

The results for the cloud of uniform composition defined in Fig. 1 are plotted in Fig. 18. They were calculated with  $\omega_t$ ,  $\omega_1$  and  $\omega_2$  equal to 1, 20 and 50 mrad. As shown, the solution fits the true  $\alpha_s^+$  profile very well, absolute local errors are less than  $0.1 \text{ km}^{-1}$  or about 3% of the average true  $\alpha_s^+$ . The cloud-integrated  $\alpha_s^+$ , or forward-scattering optical depth, agrees with the true value within 1%.

The results for the cloud defined in Fig. 2 are shown in Fig. 19. Despite important variations in albedo and backscatter-to-extinction ratio, the agreement with the true  $\alpha_s^+$  is still acceptable, local errors are less than 10%. The solutions for the more complex cloud structures illustrated in Figs. 3 and 4 are given in Figs. 20 and 21, respectively. Again, the agreement is very good with some exceptions at points where the albedo and  $\beta/\alpha_e$  change abruptly. The cumulative effects of the solution errors on the calculated cloud optical depth are less than 10-15%. In all cases, the true profiles are well reproduced by the solutions.

As discussed previously, the proposed multiscattering technique requires that the lidar return at the smallest field of view  $\omega_t$  be dominated by single backscatterings. However, at very large optical depths, the lidar signal at  $\omega_t$  may be contaminated by multiple scatterings. The solution obtained for the cloud defined in Fig. 1 with the extinction profile multiplied by a factor of 2 is drawn in Fig. 22. The calculations were performed with  $\omega_t$ ,  $\omega_1$  and  $\omega_2$  equal to 1, 20 and 50 mrad as for the examples given in Figs. 18-21. It is shown that the solution fails to reach the high scattering coefficient value at the cloud center and that it remains below the true  $\alpha_s^+$  profile from that point on. However, the solution does not diverge and the profile has approximately the right shape.

The results of Fig. 22 indicate that the multiscattering lidar solution method becomes subject to important errors for optical depths greater than about 4. Although this limit is expected to vary with the nature of the aerosols and the profile of the extinction coefficient, it is not expected that the method defined by eqs. 23-25 will remain accurate beyond optical depths of the order of 4. This is similar to the limit found in the preceding chapter for the single-scattering inversion method under optimal conditions of known boundary value and  $\beta/\alpha_e$  profile. This is not surprising since the requirement on  $P(R, \omega_t)$ , namely that it is not significantly affected by multiple scatterings, is the same as for the validity of the single-scattering lidar equation. A more sophisticated algorithm involving measurements at more than three fields of view could possibly be defined to extend the range of applicability. However, it is questionable whether meaningful lidar measurements can be carried out at optical depths greater than 4.

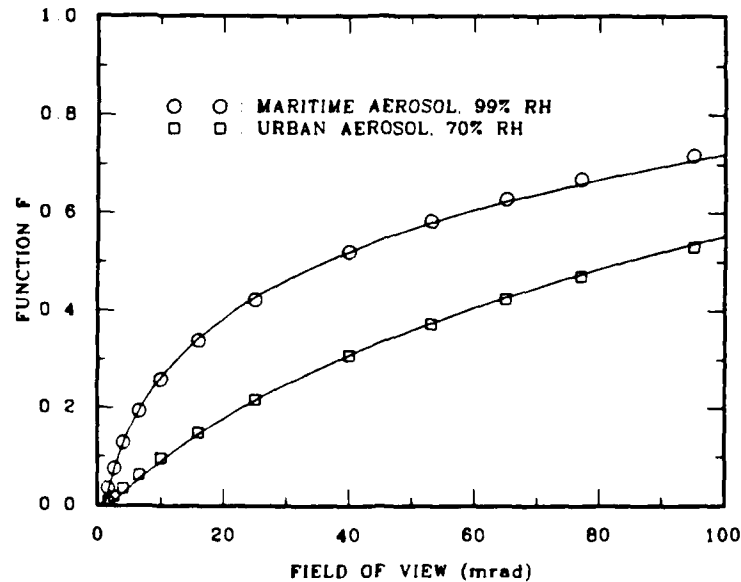


FIGURE 16 - Function  $f(\omega, \omega_t)$  defined in eq. 21 calculated for the generic models of maritime aerosol at 99% relative humidity and urban aerosol at 70% relative humidity (Ref. 11). The wavelength is  $1.06 \mu\text{m}$ . The symbols are calculations with the propagation model of Ref. 10 and the continuous curve represents empirical fit of eq. 22.  $k = 1.34$  for maritime aerosol and  $2.42$  for urban aerosol;  $b = 2.6$  in both cases.

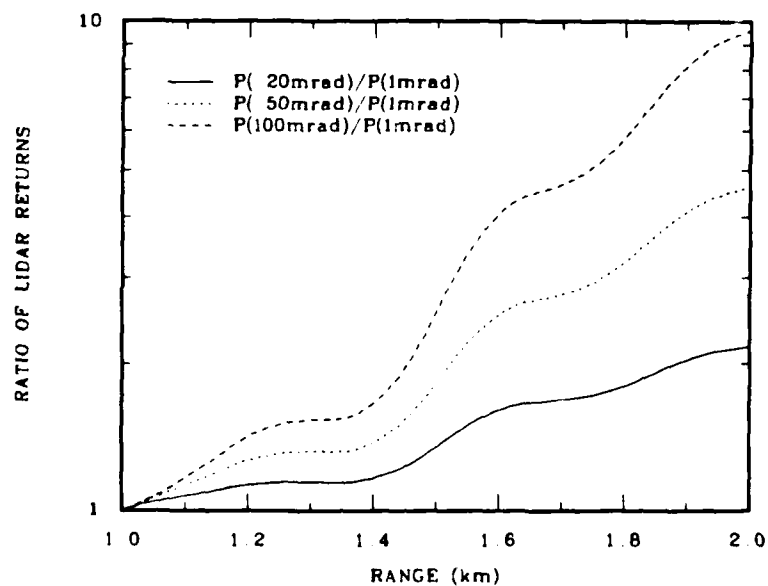


FIGURE 17 - Examples of ratios of lidar signals at different fields of view calculated from the cloud defined in Fig. 3.

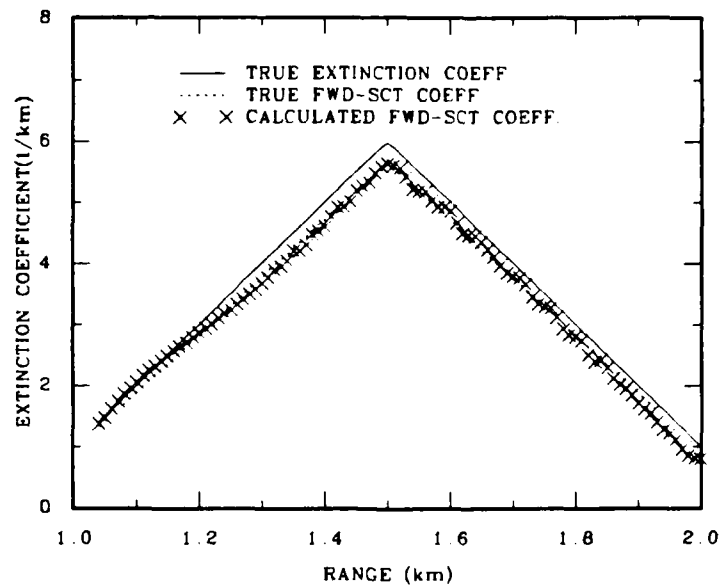


FIGURE 18 - Solutions for the forward-scattering (FWD-SCT) aerosol coefficient calculated with the multiscattering lidar inversion algorithm for the cloud defined in Fig. 1.

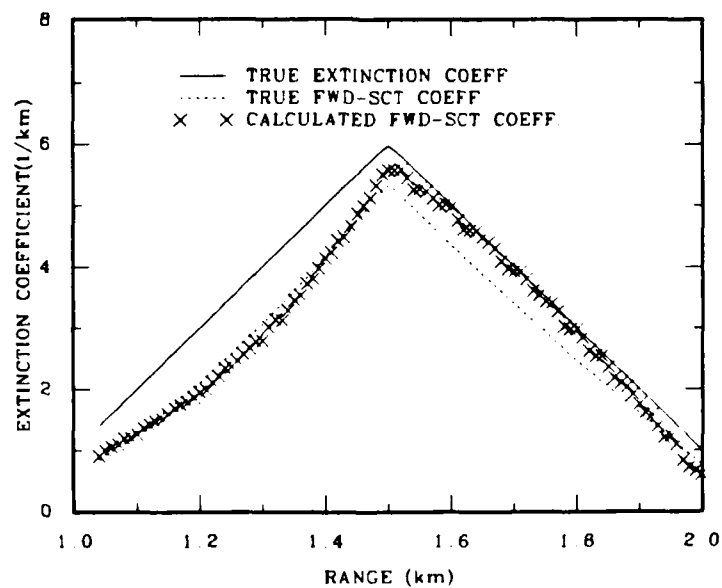


FIGURE 19 - Same as Fig. 18 but for the cloud defined in Fig. 2.

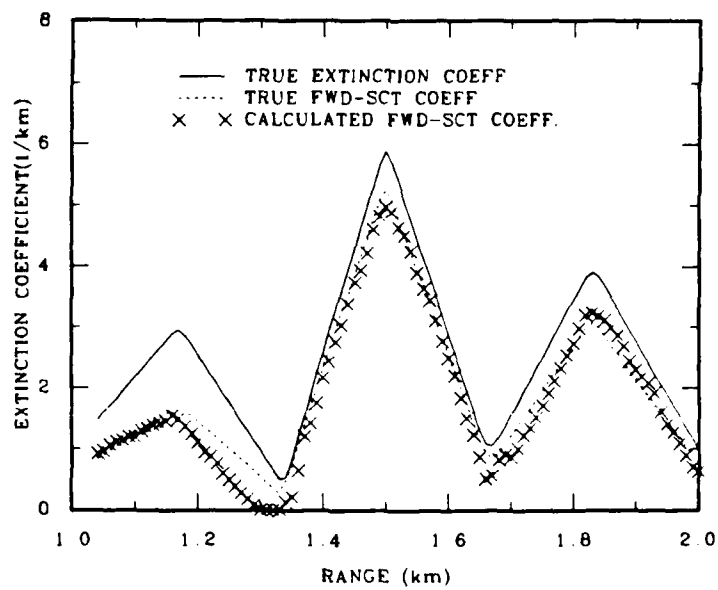


FIGURE 20 - Same as Fig. 18 but for the cloud defined in Fig. 3.

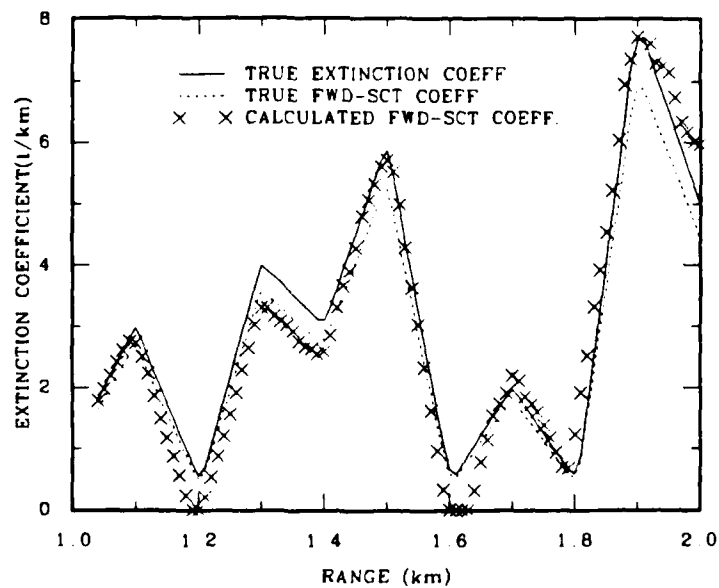


FIGURE 21 - Same as Fig. 18 but for the cloud defined in Fig. 4.

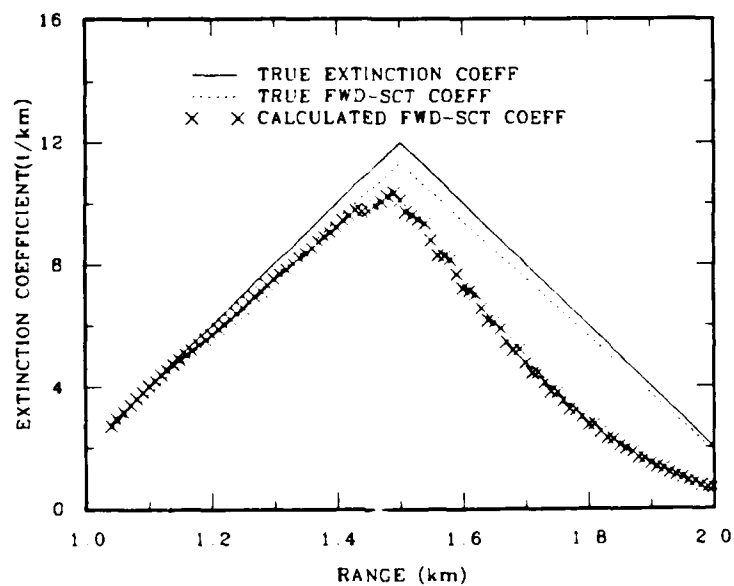


FIGURE 22 - Same as Fig. 18 but for doubled aerosol concentration or doubled extinction coefficient.

## 5.0 SUMMARY AND CONCLUSIONS

This report has described a new lidar inversion method for the determination of the aerosol scattering coefficient. Its principal characteristic is the use of the information contained in the multi-scattering contributions of the measured lidar returns. The method requires neither a boundary value nor a backscatter-to-extinction relation. Performance proved to be more consistent than with the standard single-scattering lidar method for the same simulated applications.

The simulated lidar signals were generated with the multiscattering propagation model of Ref. 9. Inhomogeneous clouds were constructed from the generic maritime, rural and urban aerosol models developed by the Air Force Geophysics Laboratory (Ref. 11). These models were designed from measurements and they represent adequately a wide variety of atmospheric conditions. Range-resolved lidar signals were calculated as functions of the receiver field of view.

The single-scattering lidar inversion algorithm based on the specification of the boundary value at the front end of the cloud was found to be inadequate under all conditions studied. The solutions for the aerosol extinction coefficient either diverged to infinity or quickly fell off to zero. On the other hand, the inversion method that integrates from the backside of the cloud onward remained stable in all cases. However, the results showed that the calculated extinction coefficient can be seriously affected by uncertainties in the boundary value and in the backscatter-to-extinction ratio for clouds of inhomogeneous composition.

The proposed multiscattering lidar inversion method requires that the range-gated lidar signals be measured simultaneously at three fields of view. One field of view is small and corresponds to the

standard design where the receiver stares only at the volume probed by the unscattered transmitter beam; the other two must be chosen just wide enough for the differences due to multiple scatterings to be measurable with sufficient accuracy. The aerosol scattering phase function must be sufficiently peaked forward for these fields of view to be kept within practical limits. The inputs to the solution method are the ratios of the lidar signals at the different fields of view. The algorithm involves only algebraic equations and is very similar to the well-known slope method. It requires the calibration of one system constant: the parameter  $b$  in eq. 22. The calculation results fit very well the true profiles in all cases. The agreement was consistently better than for the single-scattering solutions except where the exact boundary value and the exact backscatter-to-extinction profiles were given, in which case performances are similar. The algorithm could still be improved, particularly the determination of the field-of-view function  $f(\omega, \omega_t)$  defined in eq. 21.

The method solves for the aerosol forward-scattering coefficient defined by eq. 7 and not for the extinction coefficient, but the two are related through a proportionality constant. For atmospheric aerosols and operating wavelengths in the visible and infrared, the proportionality constant is approximately equal to the aerosol single-scattering albedo; it is actually smaller, by 5-10% at the most. Except for highly absorbing aerosols, the differences between the forward-scattering and extinction coefficients are probably within the experimental errors.

With the standard single-scattering solution method, the tactical use of lidar for the determination of the atmospheric aerosol optical and infrared parameters is seriously hindered by the need for advanced knowledge of a boundary value at the far end of the lidar range and of the profile of the backscatter-to-extinction ratio. The

proposed multiscattering lidar inversion technique eliminates these difficulties. The additional information is extracted from the multiscattering contributions through simultaneous measurements of the lidar returns at three fields of view. The aerosol forward-scattering coefficient is thus determined from lidar data only, independently of a boundary value and of the backscatter-to-extinction profile. Under such conditions, the use of lidar as a tactical aid to provide reliable aerosol data would be feasible. Of course, the technique needs experimental validation. Calculations have shown that receiver fields of view in the range of 1, 20 and 50 mrad (half angle) should constitute a workable design for atmospheric aerosols.

6.0 REFERENCES

1. Klett, J.D., "Stable Analytical Inversion Solution for Processing Lidar Returns", Appl. Opt., Vol. 20, pp. 211-220, 1981.
2. Klett, J.D., "Lidar Inversion with Variable Backscatter/Extinction Ratios", Appl. Opt., Vol. 24, pp. 1638-1643, 1985.
3. Hughes, H.G., Stephens, D.H. and Ferguson, J.A., "Sensitivity of a Lidar Inversion Algorithm to Parameters Relating Atmospheric Backscatter and Extinction", NOSC TD 695, Naval Ocean Systems Center, San Diego, Cal., April 1984, UNCLASSIFIED
4. Hughes, H.G., Ferguson, J.A. and Stephens, D.H., "Sensitivity of a Lidar Inversion Algorithm to Parameters and Extinction", Appl. Opt., Vol. 24, pp. 1609-1613, 1985.
5. Bissonnette, L.R., "Sensitivity Analysis of Lidar Inversion Algorithms", Appl. Opt., Vol. 25, No. 13, pp. 2122-2125, 1986.
6. Sassen, K.S. and Petrilla, R.L., "Lidar Depolarization from Multiple Scattering in Marine Stratus Clouds", Appl. Opt., Vol. 25, pp. 1450-1459, 1986.
7. Lindberg, J.D., Lentz, W.J., Measure, E.M. and Rubio, R., "Lidar Determination of Extinction in Stratus Clouds", Appl. Opt., Vol. 23, No. 13, pp. 2172-2177, 1984.
8. Kunz, G., "Survey of the Netherlands Contribution to the European Vertical Structure Experiment at Cardington (UK) from 16 to 29 January 1983", Physics and Electronics Laboratory TNO, Report IR1986-19, 1986, UNCLASSIFIED
9. Bissonnette, L.R., "Laser Forward- and Backscattering in Particulate Media", DREV R-4351/85, March 1985, UNCLASSIFIED
10. Bissonnette, L.R., "Multiple-Scattering Laser Propagation Model and Comparison with Laboratory Measurements", DREV R-4422/86, September 1986, UNCLASSIFIED
11. Shettle, E.P. and Fenn, R.W., "Models for the Aerosols of the Lower Atmosphere and the Effects of Humidity Variations on Their Optical Properties", AFGL-TR-79-0214, Air Force Geophysics Laboratory, Hanscom AFB, Massachusetts, September 1979, UNCLASSIFIED

DREV R-4430/86 (UNCLASSIFIED)

Research and Development Branch, DND, Canada.  
DREV, P.O. Box 8800, Courcellette, Que. G0A 1R0

"Multiscattering Lidar Method for Determining Optical Parameters of Aerosols"  
by L.R. Blasonnette

A new lidar technique is proposed for determining aerosol optical parameters. It consists in recording the lidar returns at three fields of view to measure the differences caused by multiple scatterings. The inversion algorithm uses that information to obtain the aerosol forward-scattering coefficient through simple algebraic formulas. Sample solutions are calculated for simulated lidar signals and compared with the results derived from the standard single-scattering lidar equation. The agreement with the true values is very good and performance is consistently better than, or at least as good as, that of the single-scattering method. The proposed technique requires neither a boundary value nor a backscatter-to-extinction relation, which makes such lidar measurements completely self-sufficient for the remote determination of the range-resolved forward-scattering coefficient of atmospheric aerosols.

DREV R-4430/86 (UNCLASSIFIED)

Research and Development Branch, DND, Canada.  
DREV, P.O. Box 8800, Courcellette, Que. G0A 1R0

"Multiscattering Lidar Method for Determining Optical Parameters of Aerosols"  
by L.R. Blasonnette

A new lidar technique is proposed for determining aerosol optical parameters. It consists in recording the lidar returns at three fields of view to measure the differences caused by multiple scatterings. The inversion algorithm uses that information to obtain the aerosol forward-scattering coefficient through simple algebraic formulas. Sample solutions are calculated for simulated lidar signals and compared with the results derived from the standard single-scattering lidar equation. The agreement with the true values is very good and performance is consistently better than, or at least as good as, that of the single-scattering method. The proposed technique requires neither a boundary value nor a backscatter-to-extinction relation, which makes such lidar measurements completely self-sufficient for the remote determination of the range-resolved forward-scattering coefficient of atmospheric aerosols.

DREV R-4430/86 (UNCLASSIFIED)

Research and Development Branch, DND, Canada.  
DREV, P.O. Box 8800, Courcellette, Que. G0A 1R0

"Multiscattering Lidar Method for Determining Optical Parameters of Aerosols"  
by L.R. Blasonnette

A new lidar technique is proposed for determining aerosol optical parameters. It consists in recording the lidar returns at three fields of view to measure the differences caused by multiple scatterings. The inversion algorithm uses that information to obtain the aerosol forward-scattering coefficient through simple algebraic formulas. Sample solutions are calculated for simulated lidar signals and compared with the results derived from the standard single-scattering lidar equation. The agreement with the true values is very good and performance is consistently better than, or at least as good as, that of the single-scattering method. The proposed technique requires neither a boundary value nor a backscatter-to-extinction relation, which makes such lidar measurements completely self-sufficient for the remote determination of the range-resolved forward-scattering coefficient of atmospheric aerosols.

DREV R-4430/86 (UNCLASSIFIED)

Research and Development Branch, DND, Canada.  
DREV, P.O. Box 8800, Courcellette, Que. G0A 1R0

"Multiscattering Lidar Method for Determining Optical Parameters of Aerosols"  
by L.R. Blasonnette

A new lidar technique is proposed for determining aerosol optical parameters. It consists in recording the lidar returns at three fields of view to measure the differences caused by multiple scatterings. The inversion algorithm uses that information to obtain the aerosol forward-scattering coefficient through simple algebraic formulas. Sample solutions are calculated for simulated lidar signals and compared with the results derived from the standard single-scattering lidar equation. The agreement with the true values is very good and performance is consistently better than, or at least as good as, that of the single-scattering method. The proposed technique requires neither a boundary value nor a backscatter-to-extinction relation, which makes such lidar measurements completely self-sufficient for the remote determination of the range-resolved forward-scattering coefficient of atmospheric aerosols.

CRDW R-4430/86 (SANS CLASSIFICATION)

Bureau - Recherche et Développement, MDN, Canada.  
CRDV, C.P. 8800, Courcellette, Qué. G0A 1R0

"Méthode lidar basée sur la diffusion multiple pour déterminer les paramètres optiques des aérosols"  
par L.R. Bissonnette

Une nouvelle technique lidar pour la détermination de paramètres optiques des aérosols est proposée. Elle consiste à enregistrer les rétrodiffusions lidar sous trois champs de vision angulaire pour mesurer les différences provenant des diffusions multiples. L'algorithme d'inversion utilise ces données pour obtenir par des opérations algébriques simples le coefficient de diffusion vers l'avant des aérosols. Des exemples de calcul sont effectués pour des signaux lidar simulés et comparés aux résultats obtenus à partir de l'équation du lidar en diffusion simple. Le recoupement avec les valeurs exactes est très bon et les performances sont meilleures ou du moins aussi bonnes que celles de la méthode de diffusion simple. La méthode suggérée requiert ni valeur aux limites ni relation entre les coefficients d'extinction et de rétrodiffusion, ce qui la rend tout à fait autosuffisante pour déterminer à distance la distribution spatiale du coefficient de diffusion vers l'avant des aérosols atmosphériques.

CRDW R-4430/86 (SANS CLASSIFICATION)

Bureau - Recherche et Développement, MDN, Canada.  
CRDV, C.P. 8800, Courcellette, Qué. G0A 1R0

"Méthode lidar basée sur la diffusion multiple pour déterminer les paramètres optiques des aérosols"  
par L.R. Bissonnette

Une nouvelle technique lidar pour la détermination de paramètres optiques des aérosols est proposée. Elle consiste à enregistrer les rétrodiffusions lidar sous trois champs de vision angulaire pour mesurer les différences provenant des diffusions multiples. L'algorithme d'inversion utilise ces données pour obtenir par des opérations algébriques simples le coefficient de diffusion vers l'avant des aérosols. Des exemples de calcul sont effectués pour des signaux lidar simulés et comparés aux résultats obtenus à partir de l'équation du lidar en diffusion simple. Le recoupement avec les valeurs exactes est très bon et les performances sont meilleures ou du moins aussi bonnes que celles de la méthode de diffusion simple. La méthode suggérée requiert ni valeur aux limites ni relation entre les coefficients d'extinction et de rétrodiffusion, ce qui la rend tout à fait autosuffisante pour déterminer à distance la distribution spatiale du coefficient de diffusion vers l'avant des aérosols atmosphériques.

CRDW R-4430/86 (SANS CLASSIFICATION)

Bureau - Recherche et Développement, MDN, Canada.  
CRDV, C.P. 8800, Courcellette, Qué. G0A 1R0

"Méthode lidar basée sur la diffusion multiple pour déterminer les paramètres optiques des aérosols"  
par L.R. Bissonnette

Une nouvelle technique lidar pour la détermination de paramètres optiques des aérosols est proposée. Elle consiste à enregistrer les rétrodiffusions lidar sous trois champs de vision angulaire pour mesurer les différences provenant des diffusions multiples. L'algorithme d'inversion utilise ces données pour obtenir par des opérations algébriques simples le coefficient de diffusion vers l'avant des aérosols. Des exemples de calcul sont effectués pour des signaux lidar simulés et comparés aux résultats obtenus à partir de l'équation du lidar en diffusion simple. Le recoupement avec les valeurs exactes est très bon et les performances sont meilleures ou du moins aussi bonnes que celles de la méthode de diffusion simple. La méthode suggérée requiert ni valeur aux limites ni relation entre les coefficients d'extinction et de rétrodiffusion, ce qui la rend tout à fait autosuffisante pour déterminer à distance la distribution spatiale du coefficient de diffusion vers l'avant des aérosols atmosphériques.

CRDW R-4430/86 (SANS CLASSIFICATION)

Bureau - Recherche et Développement, MDN, Canada.  
CRDV, C.P. 8800, Courcellette, Qué. G0A 1R0

"Méthode lidar basée sur la diffusion multiple pour déterminer les paramètres optiques des aérosols"  
par L.R. Bissonnette

Une nouvelle technique lidar pour la détermination de paramètres optiques des aérosols est proposée. Elle consiste à enregistrer les rétrodiffusions lidar sous trois champs de vision angulaire pour mesurer les différences provenant des diffusions multiples. L'algorithme d'inversion utilise ces données pour obtenir par des opérations algébriques simples le coefficient de diffusion vers l'avant des aérosols. Des exemples de calcul sont effectués pour des signaux lidar simulés et comparés aux résultats obtenus à partir de l'équation du lidar en diffusion simple. Le recoupement avec les valeurs exactes est très bon et les performances sont meilleures ou du moins aussi bonnes que celles de la méthode de diffusion simple. La méthode suggérée requiert ni valeur aux limites ni relation entre les coefficients d'extinction et de rétrodiffusion, ce qui la rend tout à fait autosuffisante pour déterminer à distance la distribution spatiale du coefficient de diffusion vers l'avant des aérosols atmosphériques.